Further Investigations into Connection Repeatability of Waveguide Devices at Frequencies from 750 GHz to 1.1 THz

N M Ridler[1] and R G Clarke[2]

[1]National Physical Laboratory, UK, nick.ridler@npl.co.uk

[2]University of Leeds, UK, r.g.clarke@leeds.ac.uk

***Abstract*—This paper describes some further investigations into the connection repeatability for waveguide devices in the WM-250 (WR-01) waveguide size over the recommended frequency range of 750 GHz to 1.1 THz. This work follows previous work on this subject that was presented at the 82nd ARFTG conference in November 2013. As with the earlier investigation, three devices have been investigated – an offset short-circuit, a flush short-circuit, and a near-matched load. These devices can be used as calibration standards for Vector Network Analyzers (VNAs), and so can be found in VNA calibration kits. On this occasion, the aperture of each device was inverted (i.e. rotated through 180º) between the repeated disconnection and re-connection of the device to the VNA test port. This provides an experimental evaluation of the effect of the imperfect position of the device's flange alignment pins and holes. As before, the repeatability of the measurements is assessed using statistical techniques, in terms of the experimental standard deviation in both the real and imaginary components of the complex-valued linear reflection coefficient. The results obtained during this investigation are compared with the results obtained from the previous investigation (where flange inversion was not included as part of the disconnection and re-connection procedure for the devices).**

***Index Terms*—Measurement repeatability, Measurement standards, VNA calibration, Submillimeter-wave measurements, Measurement uncertainty**

1. INTRODUCTION

Vector Network Analyzers (VNAs) that can operate at high millimeter-wave and submillimeter-wave frequencies (i.e. 110 GHz to 1.1 THz) are now readily available as commercial systems. These VNAs use rectangular metallic waveguide as the test ports [1]. The dimensions of the waveguide apertures are very small at these frequencies – e.g. the nominal aperture dimensions for WM-250 waveguide (which operates from 750 GHz to 1.1 THz) is 250 μm × 125 μm [2]. Accurate alignment of the waveguide becomes critical at these frequencies in order to achieve electrical measurements that have an acceptable degree of reliability and repeatability. The inevitable misalignment of the waveguide (due to the imperfect waveguide flange/interface) induces both random and systematic errors into the electrical measurements. For example, random errors will be caused by the dimensional tolerances on the flange alignment mechanisms (i.e. the diameters of the dowel pins and holes). These dimensional tolerances will give rise to a lack of repeatability in the measurements. Systematic errors will be caused by the imperfect position, on the flange face, of the flange alignment mechanisms (i.e. the dowel pins and holes). These systematic errors will be present in all connections that are made for a given device and will typically be of a similar size (when connected to the same VNA test port).

An earlier connection repeatability exercise in WM-250 waveguide (reported in [3]), concentrated on assessing the random errors caused primarily by the dimensional tolerances on the flange alignment mechanisms (i.e. the diameters of the dowel pins and holes). The earlier investigation did not consider the systematic errors caused by imperfect location of these flange alignment mechanisms. The connection repeatability exercise reported in this paper extends the work presented in [3] by considering both the random and the systematic errors affecting the waveguide measurements that are caused by flange alignment imperfections. This is achieved by including connections of the waveguide devices during the repeatability exercise where the flange is inverted before being reconnected to the VNA test port. By inverting the waveguide flange, the imperfect position of the alignment pins and holes will, in principle, cause a systematic change in the electrical measurements made by the VNA. This systematic change will be present in the repeatability data sets along with the random changes caused by the tolerances on the diameters of the alignment pins and holes.

As with the previous repeatability exercise [3], the exercise presented here uses selected devices in the WM-250 (WR-01) waveguide size, operating from 750 GHz to 1.1 THz. These were the same devices that were used for the previous investigation – an offset short-circuit, a 'flush' short-circuit (i.e. a short-circuit containing no offset), and a low-reflecting (i.e. 'near-matched') load. Similar statistical analysis techniques to those used in the previous exercise are used here to enable meaningful comparisons to be made between the two repeatability exercises. Figure 1 shows a photograph of one of the flanges used during the investigation. The holes and pins used to align the flange are indicated in the photograph.

978-1-4799-4423-1/14/$31.00 ©2014 Crown

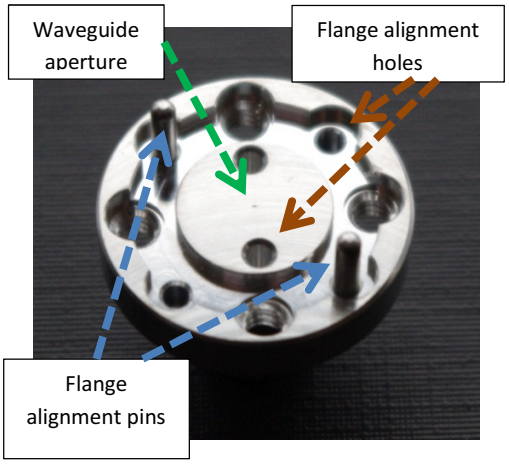

Figure 1: One of the waveguide flanges used during the connection repeatability exercise. The rectangular waveguide aperture is 250 μm × 125 μm – barely visible to the naked eye

2. METHOD

2.1 *Experimental Set-up*

The VNA system used for the investigation comprised an Agilent Technologies PNA-X VNA connected to WM-250 waveguide extender heads, manufactured by Virginia Diodes, Inc (VDI). This is the same system and set-up that was used for the previous repeatability investigation [3]. However, on this occasion, the extender head was arranged so that the waveguide test port pointed vertically upwards. This arrangement was chosen to minimize any effect due to gravity on the alignment of the waveguide flanges. As with the previous investigation, the power used to measure each Device Under Test (DUT) was around −35 dBm (0.3 μW) and the VNA's IF bandwidth was set to 30 Hz with no numerical averaging. This VNA system, shown in Figure 2, is situated in the Roger Pollard High Frequency Measurements Laboratory (this being a temperature-controlled laboratory) at the School of Electronic and Electrical Engineering, University of Leeds, UK. (Note: the vertical test port arrangement that was used for this investigation is not shown in this Figure.)

The VNA system was calibrated using a one-port 'three-known-loads' calibration technique. The 'known loads' (i.e. calibration standards) were an offset short-circuit, a 'flush' short-circuit and 'near-matched' load (from the VNA calibration kit). These same three standards were used subsequently as the DUTs for the repeatability investigation, these being the same DUTs that were used in [3].

For each flange connection orientation (i.e. either inverted or non-inverted), the complex-valued linear reflection coefficient of each DUT was measured 12 times, disconnecting and re-connecting the DUT between each re-measurement. This produced a set of 12 separate determinations of reflection coefficient for each DUT in each of the two orientations. Therefore, a total of 24 dis-connect / reconnect measurements were made for each of the three DUTs. All measurements were made from 750 GHz to 1.1 THz at regular intervals of 1.75 GHz across the band.

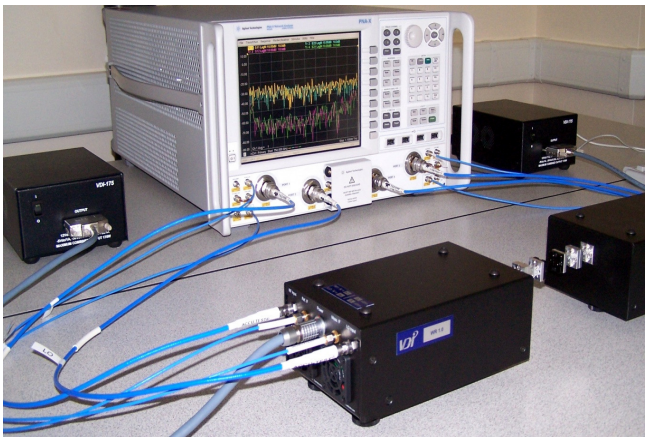

Figure 2: The 750 GHz to 1.1 THz VNA system used for the measurements

2.2 *Data Analysis*

The analysis uses calculations of the experimental standard deviation (as used previously in [3]) as the measure of variability in the observed values due to flange connection repeatability. This computation is applied separately to both the real and imaginary components of the complex-valued linear reflection coefficient. We avoid performing the analysis using the magnitude and phase components of the reflection coefficient due to problems with such calculations that have been described in [4].

Let Γ be the complex-valued linear reflection coefficient written in terms of its real, Γ_R, and imaginary, Γ_I, components as follows (with $j^2 = -1$):

$$\Gamma = \Gamma_R + j\,\Gamma_I \tag{1}$$

For n repeated determinations of Γ, the arithmetic mean of Γ_R is given by:

$$\overline{\Gamma_R} = \frac{1}{n}\sum_{i=1}^{n}\Gamma_{R_i} \tag{2}$$

and the experimental variance is given by:

$$s^2(\Gamma_{R_i}) = \frac{1}{n-1}\sum_{k=1}^{n}(\Gamma_{R_k} - \overline{\Gamma_R})^2 \tag{3}$$

The experimental standard deviation, $s(\Gamma_{R_i})$, is equal to the positive square root of $s^2(\Gamma_{R_i})$.

Similarly, the arithmetic mean of Γ_I is given by:

$$\overline{\Gamma}_I = \frac{1}{n}\sum_{i=1}^{n}\Gamma_{I_i} \tag{4}$$

and the experimental variance is given by:

$$s^2(\Gamma_{I_i}) = \frac{1}{n-1}\sum_{j=1}^{n}(\Gamma_{I_j} - \overline{\Gamma}_I)^2 \tag{5}$$

The experimental standard deviation, $s(\Gamma_{I_i})$, is equal to the positive square root of $s^2(\Gamma_{I_i})$.

For each DUT at each frequency, values of $s(\Gamma_{R_i})$ and $s(\Gamma_{I_i})$ are calculated for the following three situations:

(i) Using the 12 repeat measurements of the flange when connected in the non-inverted orientation. We use a superscript *N* to indicate this 'Non-inverted' situation – i.e. Γ_R^N for the real component, and Γ_I^N for the imaginary component;

(ii) Using the 12 repeat measurements of the flange when connected in the inverted orientation. We use a superscript *I* to indicate this 'Inverted' situation – i.e. Γ_R^I for the real component, and Γ_I^I for the imaginary component;

(iii) Using all 24 repeated measurements of the flange connected in both inverted and non-inverted orientations. We use a superscript *IN* to indicate this 'Inverted and Non-inverted' situation – i.e. Γ_R^{IN} for the real component, and Γ_I^{IN} for the imaginary component.

Since the experimental standard deviation is an *unbiased* statistical estimator, the calculated values of the experimental standard deviations for each real and imaginary component can be compared meaningfully with each other, independent of sample size, to see if the distributions for the three situations are consistent. So, we can compare the calculated values of the experimental standard deviations in the real component, $s(\Gamma_{R_i}^N)$, $s(\Gamma_{R_i}^I)$ and $s(\Gamma_{R_i}^{IN})$, and, we can compare the calculated values of the experimental standard deviations for the imaginary component $s(\Gamma_{I_i}^N)$, $s(\Gamma_{I_i}^I)$ and $s(\Gamma_{I_i}^{IN})$.

3. RESULTS

The results for each device – offset short-circuit, flush short-circuit and near-matched load – are presented as a pair of graphs showing:

(i) The calculated values of experimental standard deviations in the real component, $s(\Gamma_{R_i}^N)$, $s(\Gamma_{R_i}^I)$ and $s(\Gamma_{R_i}^{IN})$, as a function of frequency. Also shown are the experimental standard deviations obtained during the repeatability assessment in 2013 (from [3]).

(ii) The calculated values of experimental standard deviations for the imaginary component, $s(\Gamma_{I_i}^N)$, $s(\Gamma_{I_i}^I)$ and $s(\Gamma_{I_i}^{IN})$, as a function of frequency. Also shown are the experimental standard deviations obtained during the repeatability assessment in 2013 (from [3]).

Figures 3 and 4 show the results for the offset short-circuit; Figures 5 and 6 show the results for the flush short-circuit; and Figures 7 and 8 show the results for the near-matched load. Note that the vertical axes' sensitivies (i.e. scales) on these pairs of graphs differ: a full scale of 0.4 is used for the offset short-circuit graphs; a full scale of 0.2 is used for the flush short-circuit graphs; and, a full scale of 0.1 is used for the near-matched load graphs.

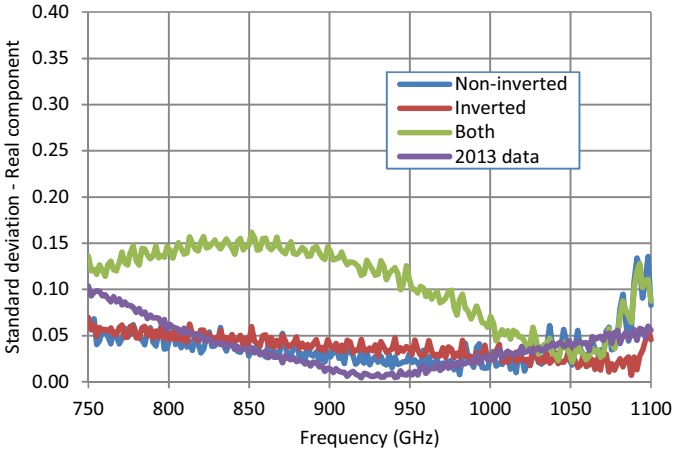

Figure 3: $s(\Gamma_{R_i}^N)$, $s(\Gamma_{R_i}^I)$ and $s(\Gamma_{R_i}^{IN})$ for the offset short-circuit. Also shown are the results from 2013

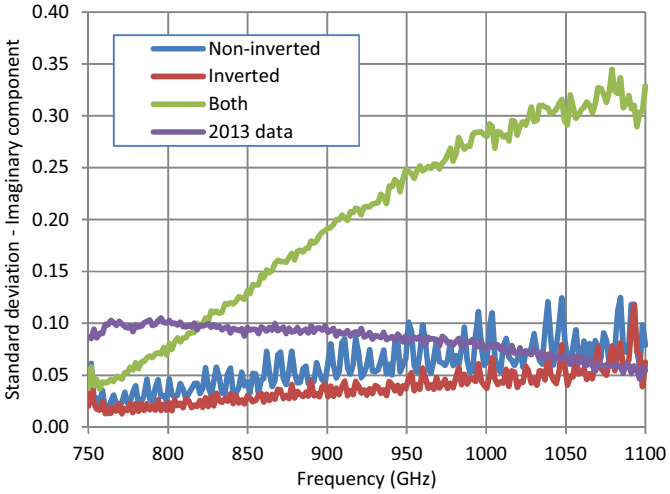

Figure 4: $s(\Gamma_{I_i}^N)$, $s(\Gamma_{I_i}^I)$ and $s(\Gamma_{I_i}^{IN})$ for the offset short-circuit. Also shown are the results from 2013

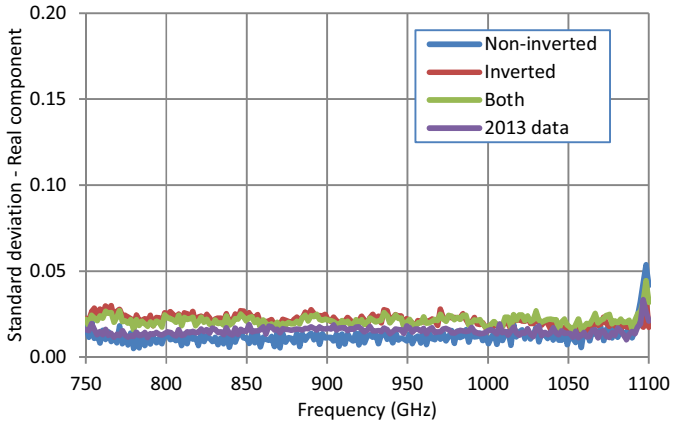

Figure 5: $s(\Gamma_{R_i}^N)$, $s(\Gamma_{R_i}^I)$ and $s(\Gamma_{R_i}^{IN})$ for the flush short-circuit. Also shown are the results from 2013

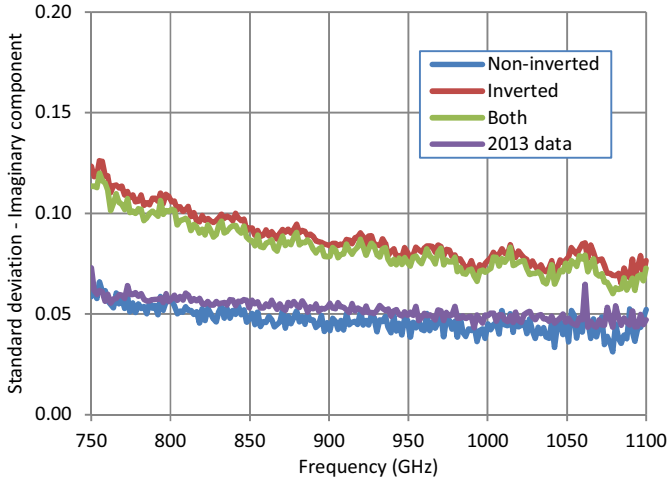

Figure 6: $s(\Gamma_{I_i}^N)$, $s(\Gamma_{I_i}^I)$ and $s(\Gamma_{I_i}^{IN})$ for the flush short-circuit. Also shown are the results from 2013

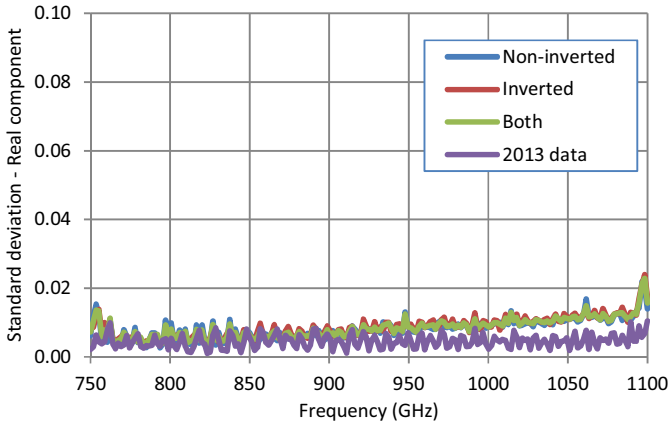

Figure 7: $s(\Gamma_{R_i}^N)$, $s(\Gamma_{R_i}^I)$ and $s(\Gamma_{R_i}^{IN})$ for the near-matched load. Also shown are the results from 2013

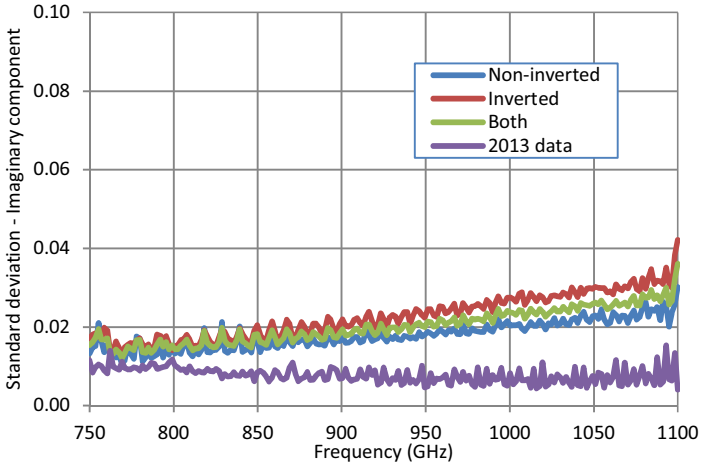

Figure 8: $s(\Gamma_{I_i}^N)$, $s(\Gamma_{I_i}^I)$ and $s(\Gamma_{I_i}^{IN})$ for the near-matched load. Also shown are the results from 2013

4. DISCUSSION

4.1 *Offset short-circuit*

By examining Figures 3 and 4, it is clear that, for both real and imaginary components, the experimental standard deviations for each flange connection orientation – i.e. non-inverted and inverted – are of a similar size (i.e. typically ≤ 0.10 across the band). These standard deviation values are also of a similar size to the values obtained during the repeatability exercise in 2013. This indicates that the amount of connection variability in the two flange orientations is of similar size. This is to be expected, since we should only be observing variability due to the dimensional tolerances of the diameters of the flange alignment pins and holes.

However, Figures 3 and 4 also show that the experimental standard deviations obtained when the data from both flange orientations are analyzed together, are significantly larger (i.e. increasing to around 0.15 for the real component, and to around 0.35 for the imaginary component) than the standard deviations for each separate flange orientation – either non-inverted or inverted. This indicates that there is a significant systematic difference between the average values of the real and imaginary components of the repeatability data for each orientation. It is expected that such a systematic difference is caused by the imperfect positioning of the flange alignment pins and holes, and so the waveguide apertures of the DUT and the VNA test port will be misaligned by different amounts, depending on the orientation used for the connection of the DUT.

We can further examine this effect by calculating the averages (i.e. arithmetic means) of the repeated connections for each flange orientation – non-inverted and inverted. The arithmetic means for the real component of the repeated non-inverted and inverted flange connections ($\bar{\Gamma}_R^N$ and $\bar{\Gamma}_R^I$,

respectively) are shown in Figure 9. Similarly, the arithmetic means for the imaginary component of the repeated non-inverted and inverted flange connections ($\bar{\Gamma}_I^N$ and $\bar{\Gamma}_I^I$, respectively) are shown in Figure 10.

Figure 9 shows differences of up to 0.30 between the mean real components of the linear reflection coefficient for the two flange orientations, and Figure 10 shows differences of up to 0.66 between the mean imaginary components of the linear reflection coefficient for the two flange orientations. These are very large differences, especially when compared to the observed experimental standard deviations for the repeatability of each flange orientation (which are typically ≤ 0.10, for both real and imaginary components, across the band).

4.2 *Flush short-circuit*

By examining Figures 5 and 6, it is clear that the experimental standard deviations for the imaginary component are significantly larger than the experimental standard deviations for the real component. This is consistent with the behavior observed during the repeatability exercise in 2013. In addition, the experimental standard deviations for inverted flange connection are larger than the experimental standard deviations for the non-inverted flange connection orientation. It is not clear why this should be, particularly as the flush short-circuit device is essentially just a flat sheet of metal and does not contain a waveguide aperture.

As with the offset short-circuit, we can calculate the arithmetic means for the real and imaginary components of the repeated non-inverted and inverted flange connections ($\bar{\Gamma}_R^N$ and $\bar{\Gamma}_R^I$, and $\bar{\Gamma}_I^N$ and $\bar{\Gamma}_I^I$, respectively). These are shown in Figures 11 and 12, respectively.

4.3 *Near-matched load*

By examining Figures 7 and 8, it is clear that the experimental standard deviations for both the real and imaginary component are of similar size (i.e. all values are less than 0.05). This is consistent with the behavior observed during the repeatability exercise in 2013. There is no clear difference between the experimental standard deviations for inverted flange connection and the non-inverted.

As with the offset and flush short-circuits, we can calculate the arithmetic means for the real and imaginary components of the repeated non-inverted and inverted flange connections ($\bar{\Gamma}_R^N$ and $\bar{\Gamma}_R^I$, and $\bar{\Gamma}_I^N$ and $\bar{\Gamma}_I^I$, respectively). These are shown in Figures 13 and 14, respectively. These Figures show that there is no significant difference between the mean real and the mean imaginary components of the linear reflection coefficient for the two flange orientations.

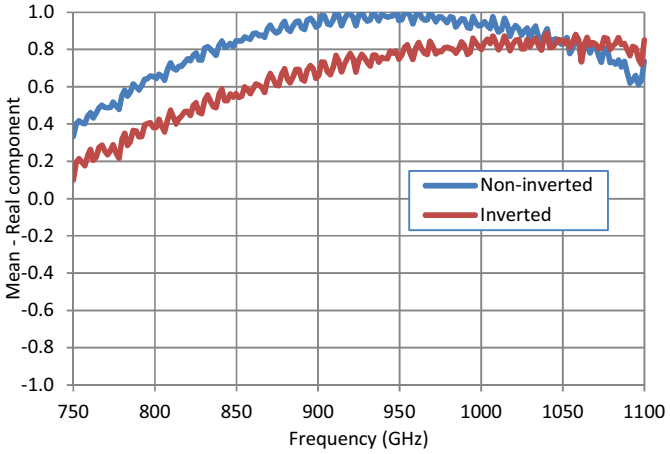

Figure 9: $\bar{\Gamma}_R^N$ and $\bar{\Gamma}_R^I$ for the offset short-circuit

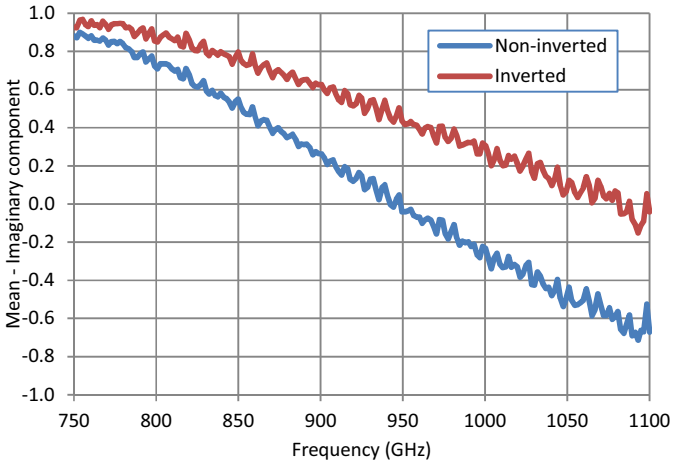

Figure 10: $\bar{\Gamma}_I^N$ and $\bar{\Gamma}_I^I$ for the offset short-circuit

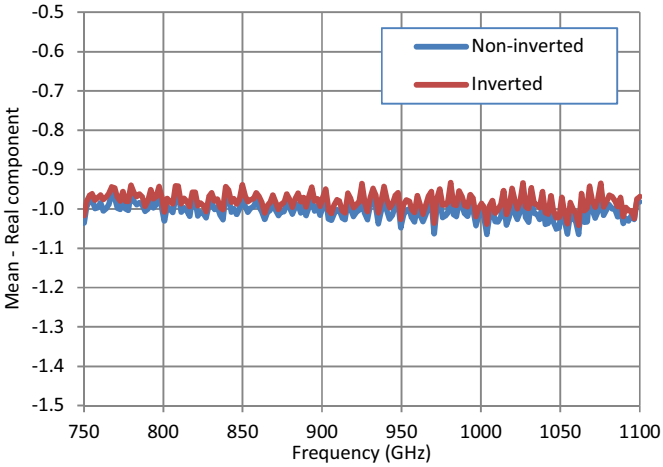

Figure 11: $\bar{\Gamma}_R^N$ and $\bar{\Gamma}_R^I$ for the flush short-circuit

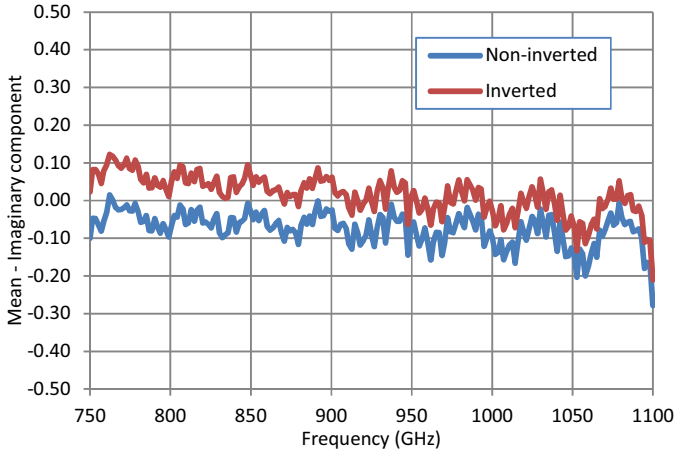

Figure 12: $\bar{\Gamma}_I^N$ and $\bar{\Gamma}_I^I$ for the flush short-circuit

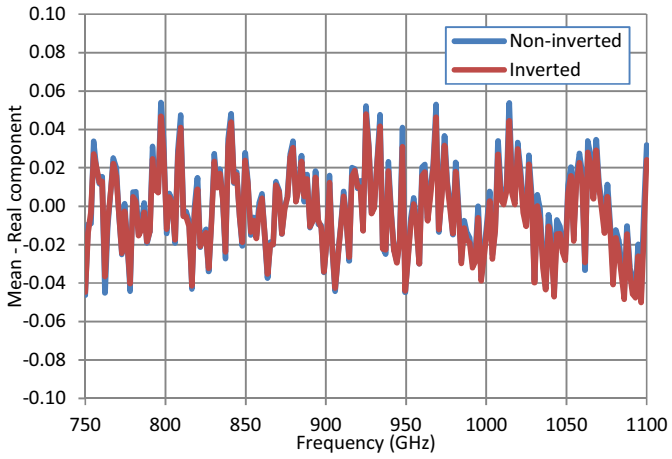

Figure 13: $\bar{\Gamma}_R^N$ and $\bar{\Gamma}_R^I$ for the near-matched load

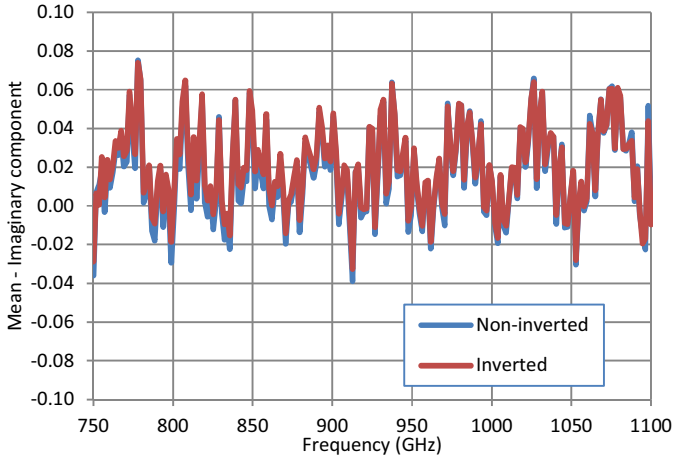

Figure 14: $\bar{\Gamma}_I^N$ and $\bar{\Gamma}_I^I$ for the near-matched load

5. SUMMARY OBSERVATIONS

We can further summarize the information for each device by recording the average observed standard deviation for each of the two flange orientations – inverted and non-inverted – for both real and imaginary components, shown in Figures 3 to 8, and compare these values with the average difference of the arithmetic means of the repeated connections for each flange orientation (shown in Figures 9 to 14), i.e. the average of ($\bar{\Gamma}_R^N - \bar{\Gamma}_R^I$), and, the average of ($\bar{\Gamma}_I^N - \bar{\Gamma}_I^I$). These summary values are shown in Table I (a), (b) and (c) for the offset short-circuit, flush short-circuit and near-matched load, respectively.

Table I (a) shows that, for both real and imaginary components, the average difference between the inverted and non-inverted connections for the offset short-circuit is much greater than the average standard deviations for both inverted and non-inverted connections. This suggests that, on this occasion, the errors due to the positional accuracy of the waveguide alignment pins and holes have a much greater impact on the electrical measurements compared with the errors due to the tolerance on the diameters of these alignment pins and holes.

Table I (b) shows that, for both real and imaginary components, the average difference between the inverted and non-inverted connections for the flush short-circuit is of a similar size to the average standard deviations for both the inverted and non-inverted connections. This suggests that, on this occasion, the errors due to the positional accuracy of the waveguide alignment pins and holes have a similar impact on the electrical measurements compared with the errors due to the tolerance on the diameters of these alignment pins and holes.

Table I (c) shows that, for both real and imaginary components, the average difference between the inverted and non-inverted connections for the near-matched load is significantly less than the average standard deviations for both the inverted and non-inverted connections. This suggests that, on this occasion, the errors due to the positional accuracy of the waveguide alignment pins and holes have less impact on the electrical measurements compared with the errors due to the tolerance on the diameters of these alignment pins and holes.

The information in Table I shows that dimensional errors in the waveguide flange alignment mechanisms generally have a different impact on the electrical measurements dependent on the type of device being measured. The indications are that high reflecting devices are more likely to be affected by the errors due to the positional accuracy of the waveguide alignment pins and holes; low reflecting devices are more likely to be affected by errors due to the tolerance on the diameters of these alignment pins and holes.

TABLE I

AVERAGE STANDARD DEVIATIONS, AND, AVERAGE DIFFERENCE BETWEEN MEANS OF INVERTED AND NON-INVERTED CONNECTIONS

(a) Offset short-circuit

Component	Average standard deviation		Average difference between inverted and non-inverted connections
	Non-inverted	Inverted	
Real	0.020	0.013	0.187
Imaginary	0.059	0.038	0.380

(b) Flush short-circuit

Component	Average standard deviation		Average difference between inverted and non-inverted connections
	Non-inverted	Inverted	
Real	0.012	0.021	0.023
Imaginary	0.047	0.088	0.090

(c) Near-matched load

Component	Average standard deviation		Average difference between inverted and non-inverted connections
	Non-inverted	Inverted	
Real	0.008	0.009	0.003
Imaginary	0.018	0.023	0.003

6. CONCLUSIONS

This paper has presented results from a waveguide flange repeatability exercise in the WM-250 waveguide size at frequencies from 750 GHz to 1.1 THz. Three devices have been studied: an offset short-circuit; a flush short-circuit; and, a near-matched load. The primary focus with this repeatability exercise has been to evaluate the effect due to changing the orientation of the DUT's flange (i.e. by inverting the flange) between multiple disconnects and reconnects of the DUT. This is in contrast to the previous repeatability exercise [3] where this type of flange inversion was deliberately not included as part of the assessment procedure.

The results from the exercise have been analyzed by observing the variability in both the real and imaginary components of the complex-valued linear reflection coefficient. For both components, the results have been summarized in terms of observed experimental standard deviations. The analysis of the results has shown that, in general, it is important to take into account errors due to both the positional accuracy of the waveguide alignment pins and holes, and, the dimensional tolerances of the diameters of these pins and holes. The type of device being measured (e.g. whether it is high-reflecting or low-reflecting) can also have an impact on the size of the errors in the electrical measurements due to the imperfections in the flange alignment mechanisms.

These considerations need to be taken into account when evaluating the uncertainty in measurements made in this waveguide size, and similar waveguide sizes, used at these submillimeter-wave frequencies.

ACKNOWLEDGEMENT

The work described in this paper was jointly funded by the European Metrology Research Programme (EMRP) Project SIB62 'HFCircuits', and, the National Measurement System Directorate of the UK government's Department for Business, Innovation and Skills. The EMRP is jointly funded by the EMRP participating countries within EURAMET and the European Union.

REFERENCES

[1] J L Hesler, Y Duan, B Foley and T W Crowe, "THz Vector Network Analyzer Measurements and Calibration", 21st International Symposium on Space Terahertz Technology, Oxford, UK, April 2010.

[2] IEEE Std 1785.1-2012, "IEEE Standard for Rectangular Metallic Waveguides and Their Interfaces for Frequencies of 110 GHz and Above—Part 1: Frequency Bands and Waveguide Dimensions", March 2013.

[3] N M Ridler and R G Clarke, "Investigating Connection Repeatability of Waveguide Devices at Frequencies from 750 GHz to 1.1 THz", *Proc. 82nd ARFTG Microwave Measurement Conference*, Columbus, OH, USA, November 2013.

[4] N M Ridler and M J Salter, "Evaluating and expressing uncertainty in complex *S*-parameter measurements", *Proc. 56th ARFTG Microwave Measurement Conference,* Boulder, CO, USA, December 2000.